IEEE Access
Multidisciplinary ⋮ Rapid Review ⋮ Open Access Journal

Received December 2, 2019, accepted December 29, 2019, date of publication January 6, 2020, date of current version January 15, 2020.

Digital Object Identifier 10.1109/ACCESS.2020.2963989

A Novel Hybrid Edge Detection Method for Polarimetric SAR Images

JUNFEI SHI, HAIYAN JIN, AND ZHAOLIN XIAO
School of Computer Science and Technology, Xi'an University of Technology, Xi'an 710048, China

Corresponding author: Junfei Shi (shijunfei1@163.com)

This work was supported in part by the National Basic Research Program (913 Program) of China under Grant 2013CB329402, in part by the National Natural Science Foundation of China under Grant 61113090, Grant 61472319, Grant 61703333, and Grant 61502382, in part by the Natural Science Foundation of Shaanxi Province under Grant 2018JQ6055 and Grant 2019JQ-740, in part by the Research Project of Shaanxi Provincial Education Department under Grant 19JK0566 and in part by the Technology Innovation Project of Xi'an University of Technology under Grant 112/256081620.

ABSTRACT The edge detection plays an important role in post-processing of PolSAR images. It is still a great challenge for extracting all the edge features and suppress speckle noises, especially when weak/strong edges appear simultaneously outside and within heterogenous areas. In this paper, a novel hybrid edge detection framework is proposed to address this problem. The proposed method is designed by fusing two initial edge detectors, which can detect complementary edge information. One is an improved polarimetric constant false alarm rate (IP_CFAR) edge detector, which can detect weak edges well, but fail to detect the edges in the heterogeneous regions. The other is the proposed weighted gradient-based (WG) detector which can detect edges in heterogeneous areas well, but loses some weak edges and produces some false edges due to the speckle noises. Secondly, based on the two detectors above, a wavelet-based hybrid edge detection method is proposed by combining their merits and suppress their shortcomings. To fuse them effectively, wavelet transformation is utilized and semantic rules are defined to extract their advantages. Moreover, a despeckling scheme is designed to suppress the false edges in the wavelet domain. Experimental results demonstrate that the proposed method outperforms the state-of-art methods in extracting both weak edges and strong edges within heterogeneous regions.

INDEX TERMS Hybrid edge detection method, improved polarimetric CFAR detector, weighted gradient-based detector, wavelet fusion.

I. INTRODUCTION

Polarimetric synthetic aperture radar (PolSAR) images [1] have been paid much attention by researchers in recent years, since they can provide more information than single-polarimetric synthetic aperture radar (SAR) images. As the prerequisite step of the image processing, PolSAR edge detection is very important, which can provide important structural information for the further object recognition [2]–[4] and image interpretation [5]–[8] of PolSAR images. However, a complex PolSAR scene usually includes both heterogenous and homogenous terrain types such as the urban areas, forests, farmlands, waters and so on. Here, the urban area and the forest are considered as the heterogenous areas, since there are obvious intensity changes within them. The farmland and waters are considered as the homogenous areas since there are weak intensity changes within them. As shown in Fig.1, in the PolSAR image of Oberpfaffenhofen area, the road and the farmland are homogenous areas and the buildings are heterogenous areas. It can be seen the road edge in the red rectangle is weak edge, and the internal changes of urban areas in the yellow rectangle is the strong edge. The target of edge detection is not only to detect the boundary between different ground objects in homogenous areas, but also the internal changes of heterogeneous areas. However, it is difficult to detect both weak edges and the edge details in the heterogeneous areas by a same detection threshold. A higher threshold will lose some weak edges, while a lower threshold will produce false edges by speckle noises.

To overcome these challenges, multiple of edge detection methods [9]–[17] have been studied for decade years. There are three major thoughts for edge detection in PolSAR images according to the literature available. 1) feature-based edge detection methods [9]–[11]. For instance,

The associate editor coordinating the review of this manuscript and approving it for publication was Krishna Kant Singh.

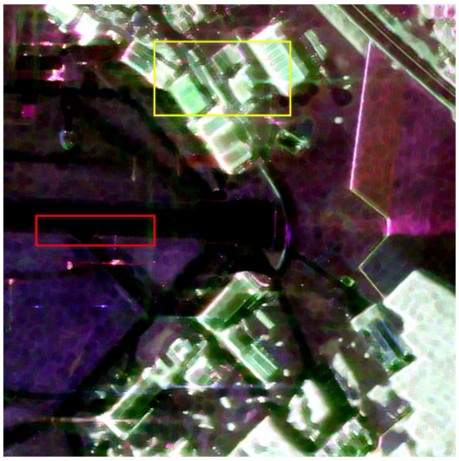

FIGURE 1. The PolSAR image on Oberpfaffenhofen.

Zhou *et al.* proposed the curvelet based edge detection method [10] to suppress the false edges. This method gave a two-scale procedure. Specifically, in the coarse scale, the curvelet transformation was utilized to obtain a coarse result as a mask to reduce speckle noises, and then an edge map was obtained within the mask in the fine scale. This method can remove false edges caused by speckle noises effectively. However, it will lose some edge details, since some weak edges with lower energy values will be removed by threshold in the coarse scale. In addition, shearlet-based edge detection methods [18], [19] can obtain sound performance in natural image. However, it was designed for natural image and didn't consider the polarimetric characteristics and speckle noise of PolSAR images. In 2013, a largest eigenvalue-based edge detection method was proposed by Deng *et al.* [12],which made fully use of the polarimetric features but had high computation complexity. Moreover, the polarimetric whitening filter (PWF)based detector [13], [14] was proposed by making use of the polarimetric information. These methods can suppress false edges well, while they may lose some edges without considering the scattering information of PolSAR data.

2) Multiple-channel fusion based methods [15]. These methods applied the single channel detector to detect edges for each polarimetric channel respectively, and then a fusion scheme was used to obtain the final edge map. However, these detectors are sensitive to speckle noises without considering the fully polarimetric information. In 2016, an improved multiscale edge detection method(IM-NSCT) [20] was proposed for PolSAR images. This method extracted edge energies by the nonsubsampled coutourlet transformation (NSCT) [21] with 8 directions in each scale, and then fused them to obtain the final edge map. This method can extract edges effectively by fusing multiscale information. However, it can still produce false edges without considering statistical characteristic [22] of PoLSAR data.

3) Statistics based edge detection methods [23]. Schou *et al.* [16] proposed the polarimetric constant false alarm rate (CFAR) detection method which made full use of the statistical distribution of PolSAR data [24] and suppressed the speckle noise effectively. However, this method failed to detect the edge details in heterogeneous terrain types such as the thin roads in the urban area. It is because that the pixels in the heterogeneous regions don't satisfy the assumption of the homogeneity any more. According to this shortcoming, Xiang *et al.* [25] proposed a new edge detector by using SIRV model [26] and Gauss-shaped filter. This method can provide more details in the heterogenous urban area. However, it needs the S matrix data which is the single look original data with abundant speckle noises. In addition, filters with fixed-shape window is limited for heterogenous areas. In 2018, Wei *et al.* [27] proposed a directional span-driven adaptive window and obtained a superior edge detection result. It also needs the S matrix data by using the SIRV model. Consequently, all these methods used filters with four directions [27]–[29], which are not enough to describe the whole edges for various terrain objects with multiple of scales and orientations.

To overcome these disadvantages, a novel edge detection framework is proposed in this paper, which firstly designs the improved polarimetric CFAR (IP_CFAR) and the weighted gradient-based detectors, and then combines them to extract their advantages. Specifically, the proposed IP_CFAR detector can detect the weak edges well with Wishart measurement, while it is difficult to detect the strong edges within heterogenous areas. On the contrary, the weighted gradient-based (WG) detector [30], owing to the anisotropic Gaussian kernel filters, can detect the sharp bright-dark variations in intensity in the heterogeneous regions well. However, it will produce some false edges due to the speckle noises [31]. Our purpose is to detect both the strong edges in the heterogenous urban area and weak edges, and remove the false edges caused by the speckle noises. Therefore, a proper fusion scheme, which can both keep the advantages of the two detectors and get rid of the shortcomings, is rather important. For this problem, some fusion functions [30], [32] have been proposed by firstly normalizing the data of the two edge energy maps. However, two sets of data are hardly to be fused accurately by comparing corresponding pixels directly since they have different distributions. Wavelet transform [33], which is an effective tool for image processing, has been widely used in image fusion [34], [35]. It can fuse two images effectively in frequency domain since wavelet coefficients in each subband have similar distribution. In addition, signal and speckle noises can be distinguished well in frequency domain.

In this paper, a new wavelet based hybrid edge detection method is proposed. This method has three novelties. 1) An IP_CFAR edge detector is designed to better detect the weak edges, and a WG detector is proposed to detect the heterogenous area well. 2) A novel edge detection framework is proposed for the first time, and it is accomplished by combining two detectors mentioned above with wavelet fusion. The proposed method can obtain both the weak edges and edge details in the heterogenous areas. 3) To extract the advantages of the two detectors and suppress their shortcomings, different fusion rules are designed in low- and high-frequency bands to both suppress the noises and enhance the edge information during wavelet fusion. Experimental results demonstrate that the proposed method can obtain sound performance in both weak edges and heterogeneous regions.

This paper is organized as follows. The motivation of image fusion is described in Section II. The proposed method is introduced in Section III. Section IV is the experimental study. The conclusion is given in Section V.

II. MOTIVATION OF IMAGE FUSION

In this paper, we fuse the IP_CFAR and gradient-based edge detectors to obtain their complementary information and remove their disadvantages.

A. MOTIVATION OF FUSING TWO DETECTORS

The IP_CFAR detector is a modified CFAR detector, and the detailed procedure of the CFAR detector can refer [16]. The CFAR detector obtained the edge energy by using the Wishart likelihood ratio, and can detect the edges well especially for the weak edges. However, it is difficult to detect the sharp intensity variations in the heterogeneous areas especially for the urban area. The reasons can be concluded into two aspects. Firstly, the pixels in the heterogenous area seldom satisfies the homogenous assumption. So, the Wishart distribution is not suitable for the heterogenous areas any more. Secondly, similar to the Ratio operator [36], [37] for SAR images, the Wishart likelihood ratio narrows the difference between two brighter pixels and amplifies the difference between two darker pixels either.

Moreover, the experimental result by the CFAR detector also verify this phenomenon as shown in Fig. 2. Figure 2(a) is the total backscattering power (SPAN) subimage of the San Francisco data. Regions 1 and 2 are the weak edge and the urban area respectively. The polarimetric energy map by CFAR detector is indicated in Fig. 2(d). It can be seen that the CFAR method can detect the weak edge in Region 1. However, it fails to detect the strong intensity variations of the urban area in Region 2, although they are easily observed by human beings.

Furthermore, since the intensity values of pixels are very different in heterogenous area, and it can be dectected by the gradient-based detector [30] from SPAN images. So, the gradient-based detector can provide complementary information for the edge-line detection. The energy map by the gradient-based detector is shown in Fig.2(e). It can be seen that the gradient-based method can detect the structure of the urban area well but not sensitive to the weak edges. In addition, some false edge energies appear in the sea and mountain areas due to speckle noises. To obtain the edge information in both heterogenous urban area and weak edges along the river, we can combine the CFAR and gradient-based detectors. Therefore, a fusion of polarimatric and gradient-based edge-line detection methods is necessary and can obtain better edge information for PolSAR images.

B. MOTIVATION OF USING WAVELET FUSION

A proper fusion scheme should keep the advantages of both detectors and get rid of their shortcomings. Some fusion functions [30], [32] have been proposed by adjusting the ranges of the two edge energy maps. These fusion methods are simple and suitable for two sets of data with similar distributions. However, when two maps are with different distributions, it is difficult to fuse them accurately.

Figs. 3(a) and (b) are the distributions of Figs.2(d) and (e) obtained by the polarimetric CFAR and gradient-based detectors respectively. It can be seen that their distributions are not similar. The distribution in Fig.3(a) is a curve with high peak and long tail, while the distribution in Fig. 3(b) is more similar to the Gaussian distribution. In [30], a fusion function is used to fuse the two data sets. However, this fusion function cannot extract both their advantages and suppress their shortcomings. It is because some important edges have low energy values in Fig.2(d), while some noises have high energies in Fig. 2(e). Fusing them directly may lose the important edges in Fig. 2(d) and remain false edges in Fig.2(e). Wavelet fusion [34], [35] is an effective way to fuse two images in frequency domain since each sub-band of two images has similar distribution. In this paper, a nonsubsampled wavelet transform [38] is utilized to obtain multiscale images with the same size. In addition, edge and non-edge information can be separated into different sub-bands. Edge information can be extracted in high-frequency bands and image energies are remained in the low frequency. Thus, different fusion rules can be defined for low- and high-frequency bands. Fig. 2(f) is the fused energy map with wavelet fusion. It can be seen that the fused result can obtain high energies in both weak edges and the urban area.

III. PROPOSED METHOD

The flowchart of the proposed hybrid edge-line detection method is shown in Fig. 4. Firstly, the IP_CFAR and WG edge detectors are proposed to detect the weak edges in the homogenous areas and strong edges within the heterogenous areas respectively. Then, a fusion scheme based on the wavelet framework is proposed to combine the two edge detection results. Thus, a fused edge map is derived by combining the advantages of both polarimatric and gradient based edge-line features.

A. IMPROVED POLARIMETRIC CFAR EDGE-LINE DETECTOR

The CFAR edge detector [16] is applied to PolSAR data since it can reduce the effect of the speckle by involving the statistical distribution of the speckle. However, the CFAR detector used filters with a single scale and four directions, which are not enough to describe the ground objects with various scales and directions. In addition, a rectangle filter with the same weight is utilized in the CFAR detector. This rectangle filter is not suitable for 2-D image smoothing, and the same weights in a filter are not reasonable since pixels

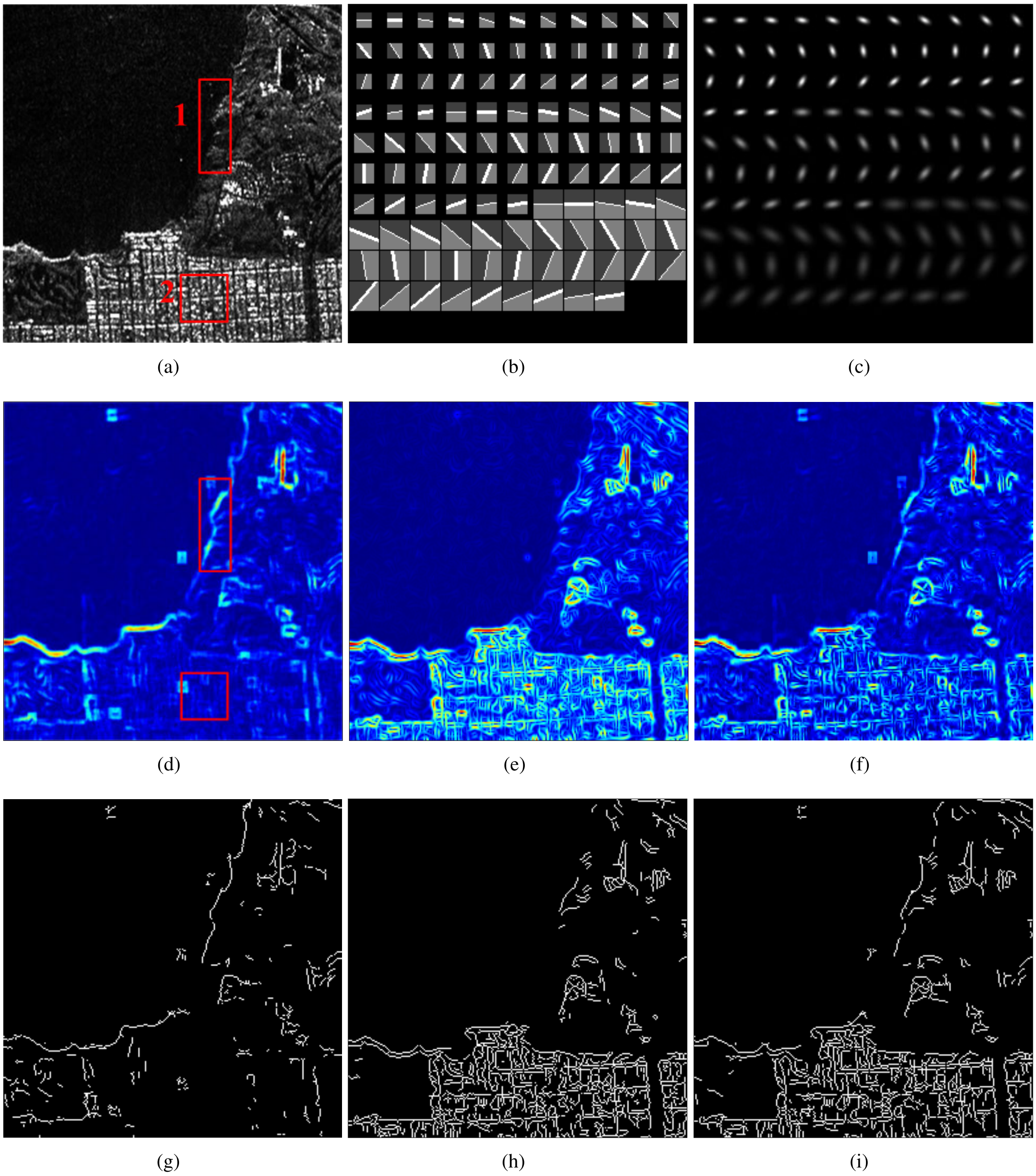

FIGURE 2. Example of the proposed edge-line detection method. (a) SPAN image of San Francisco area; (b)polarimetric edge-line filters with 3 scales and 18 directions; (c) anisotropic Gaussian kernels with 3 scales and 18 directions; (d) energy map by polarimetric CFAR detector; (e) energy map by weighted gradient detector; (f) fused energy map by the proposed method;(g) edge map by polarimetric CFAR detector; (h) edge map by weighted gradient detector; (i) edge map by the proposed method.

near the edge should have higher weights than pixels far from the edge in a filter. Therefore, we propose the IP_CFAR detector in this paper.

The IP_CFAR detector has two improvements compared with the traditional CFAR detector. One is that we design a filter configuration with multiple scales and 18 orientations instead of original filter configuration, as shown in Fig.2(b), which can better detect edges and lines. The other is an anisotropic Gaussian filter is designed instead of a rectangle shaped filter, as shown in Fig.2(c), which can provide higher weights along the edges. Moreover, a line detector is constructed by coupling of two edge detectors with a common part. Specifically, the traditional rectangle shaped edge and line filters are shown in Fig.5 (a) and (b) respectively. The edge-line filter configuration is $K_f = \{l, w, s, \theta\}$ which describes the length, width, the spacing of the filter and the orientation respectively. For edge filters, s is set to one pixel. For line detection, lines with different widths can be detected by varying s. Traditional filter configuration is single scale and four directions. Here, we construct Nf filters

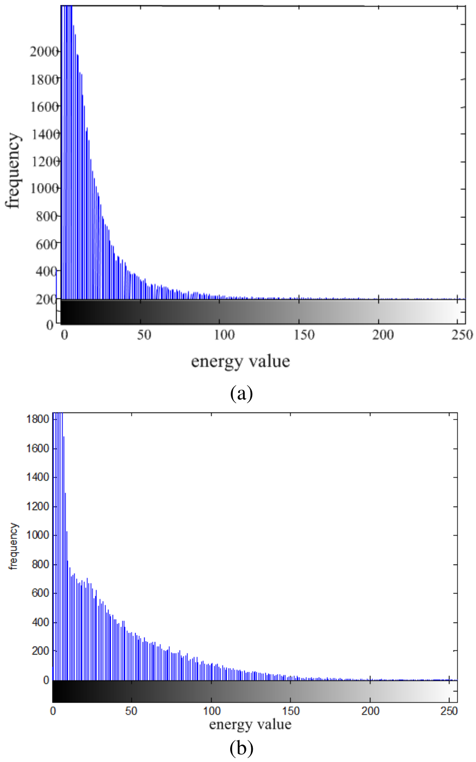

FIGURE 3. Data distribution of two energy maps. (a) Data distribution of polarimetric energy map; (b) Data distribution of gradient energy map.

with multiple scales and orientations for the edge and line detections of PolSAR images. Fig.2 (b) illustrates edge and line filters with 3 scales and 18 orientations. It is considered that the filter with 18 directions can obtain finer detection result than 4 directions. For one scale, Fig. 6(a) illustrates the rectangle shaped edge filters with 18 directions in detail. In addition, the proposed anisotropic Gaussian filters are obtained by multiplying the anisotropic Gaussian kernel to the rectangle shaped filters. The anisotropic Gaussian kernel with 18 orientations is shown in Fig. 6(b). The brighter the pixel, the larger its weight. The weight of the white pixel is 1, and the weight of the black pixel is 0. It can be seen that pixels along the orientation has larger weights, and pixels far away from the edge have smaller weights. Hence, the weighted Wishart likelihood ratio [16] is proposed to measure the similarity of two regions in a filter, which is defined as:

$$Q_{xy} = \frac{(n+m)^{p(n+m)}}{n^{pn}m^{pn}} \cdot \frac{\left|\hat{Z}_x\right|^n \left|\hat{Z}_y\right|^m}{\left|\hat{Z}_x + \hat{Z}_y\right|^{n+m}} \tag{1}$$

where

$$\hat{Z} = \frac{\sum_{i=1}^{n} w_i C_i}{\sum_{i=1}^{n} w_i} \tag{2}$$

where $\hat{Z}_x$ is the average covariance matrix in region x, C_i is the covariance matrix of the ith pixel in a region. n and m are the number of looks of the two regions in a filter respectively. p is the number of channels, and generally $p = 3$ under the reciprocity assumption [39]. w_i is the anisotropic Gaussian kernel weight. It is used to average the covariance matrix in a filter. The anisotropic Gaussian kernel for edge and line filters are defined as:

$$w(x, y) = \frac{1}{\sqrt{2\pi}\sigma_x \sqrt{2\pi}\sigma_y} \exp\left(-\left(\frac{x^2}{2\sigma_x^2} + \frac{y^2}{2\sigma_y^2}\right)\right) \tag{3}$$

where w is the anisotropic Gaussian kernel weight for pixel (x, y). σ_x and σ_y are the length and width of the filter window. Thus,for each filter configuration, the edge and line energies of a pixel are given by:

$$E_{edge} = max\left\{-2\rho logQ_{12}\right\}_{Nf} \tag{4}$$

$$E_{line} = max\left\{min\left\{-2\rho logQ_{12}, -2\rho logQ_{13}\right\}\right\}_{Nf} \tag{5}$$

and

$$\rho = 1 - \frac{2p^2 - 1}{6p}\left\{\frac{1}{n} + \frac{1}{m} - \frac{1}{n+m}\right\} \tag{6}$$

where Q_{ij} is Wishart likelihood ratio, and Nf is the number of filters which are determined by the number of scales and orientations. E_{edge} and E_{line} are edge and line energy values respectively. p is the number of channels, and generally $p = 3$ under the reciprocity assumption [39]. ρ is defined in Eq. (6) and can compute the probability of finding a smaller value of E_{edge} by the test statistic method [40]. The detail procedure can be seen in [16], [40]. According to Eq. (4), it can be seen that the edge energy is increasing with the decreasing Wishart likelihood ratio. Eq. (5) shows a line object can be detected when two edges appear with high energies in both sides of the central region. The maximum energy of a PolSAR image is obtained by comparing the energy value E in each scale and orientation.

To verify the performance improvement of the proposed IP_CFAR detector, we compare the IP_CFAR and CFAR detectors by two PolSAR images in Fig.7. The first column is the original PolSAR images, and the second and third columns are the edge-line energies by the CFAR and IP_CFAR detectors respectively. It can be seen that the proposed IP_CFAR method can not only detect more edge details in the urban areas, but also provide more accurate detection of weak edges than traditional CFAR detector.

B. WEIGHTED GRADIENT EDGE-LINE DETECTION FOR POLARIMETRIC SAR IMAGE

The IP_CFAR detector can detect weak edges well by Wishart likelihood ratio. However, it is difficult to detect the strong intensity changes in the heterogenous areas. In order to better detect the edge details in the heterogenous urban area, a weighted gradient-based(WG) edge-line detection method is proposed for the PolSAR image. Firstly, a refined Lee filter [41] is applied to PolSAR data to reduce the speckle noise. Then, to utilize the polarimetric information, we use

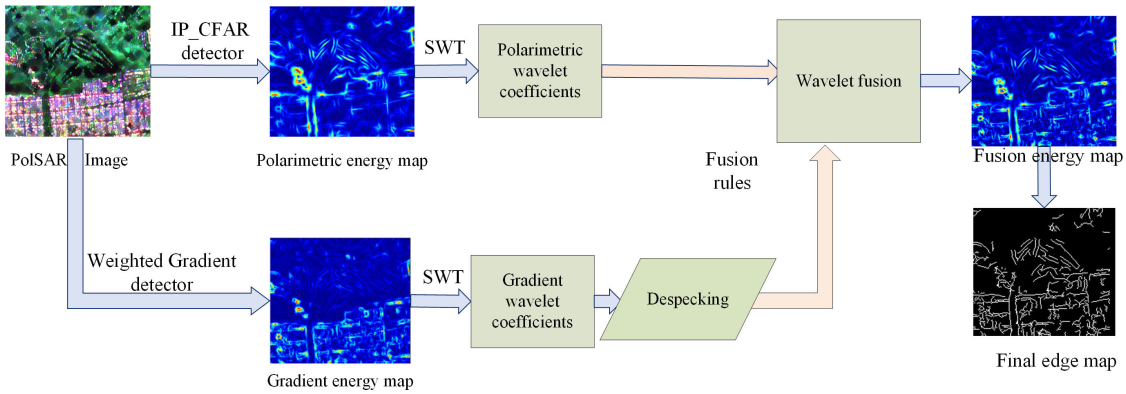

FIGURE 4. Procedure of the proposed edge-line detection method for PolSAR images.

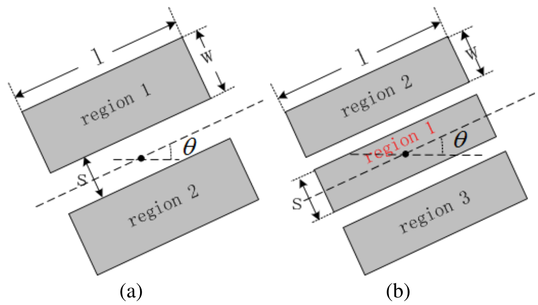

FIGURE 5. The rectangle shaped edge and line filters. (a) The rectangle shaped edge filter; (b) The rectangle shaped line filter.

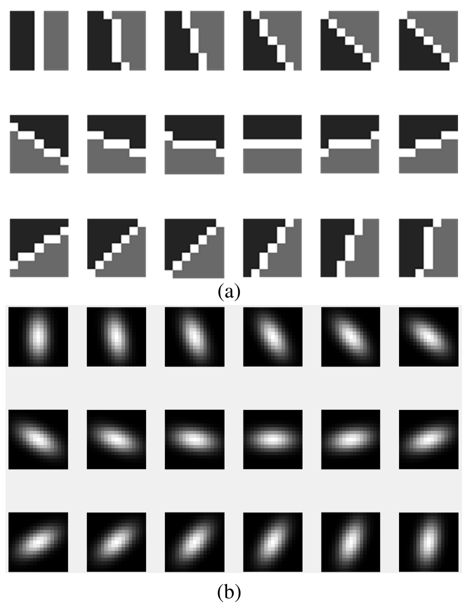

FIGURE 6. The edge filters and anisotropic Gaussian kernel filters with 18 orientations. (a) The edge filters with 18 orientations; (b) The anisotropic Gaussian kernel with 18 orientations.

the coherency matrix T [32] to calculate the gradient diffidence. The coherency matrix T is a complex conjugate symmetric matrix and defined as [42]:

$$T = \begin{pmatrix} T_{11} & T_{12} & T_{13} \\ T_{21} & T_{22} & T_{23} \\ T_{31} & T_{32} & T_{33} \end{pmatrix} \tag{7}$$

To compute gradient conveniently, we convert the coherency matrix T [42] to a nine-dimension vector V, defined as:

$$V = \{T_{11}, T_{22}, T_{33}, real(T_{12}), img(T_{12}), real(T_{13}), \\ img(T_{13}), real(T_{23}), img(T_{23})\} \tag{8}$$

where the $real(.)$ and $img(.)$ represent the real and imaginary component operations respectively.

According to the vector V, we define the WG edge-line detector for the PolSAR image. The anisotropic Gaussian filters are defined, and the Euclidean distance is used to measure the gradient difference. Since the PolSAR data vary dramatically and are mostly close to zero, a logarithmic transformation is applied to reduce the variation. In addition, for the closed double edges in PolSAR image, a line can be detected with the line filters. The weighted gradient-based edge and line detectors are defined as:

$$G_{edge} = \log || \sum_{i=1}^{n} w_i V_i - \sum_{j=1}^{m} w_j V_j ||_2 \tag{9}$$

$$G_{line} = \min\{G_{edge}^{12}, G_{edge}^{13}\} \tag{10}$$

where m and n are the pixel numbers of region 1 and 2 respectively in the edge filter as shown in Fig.5 (a). V_i is the vector of the coherency matrix of the ith pixel, and w_i is the anisotropic Gaussian weight of the ith pixel. G_{edge} and G_{line} are the edge and line gradient responses respectively. The line gradient response is defined as the minimum value of two closed edge gradient values as shown in Fig.5 (b).

To test the superiority of the proposed weighted gradient-based detector, the comparison experiments are taken on two real PolSAR images, and the detection results by WG and traditional gradient-based detectors are shown in Fig. 8. It is noted that traditional gradient-based detector also use the vector V to compute the edge-line energies.

C. HYBRID EDGE-LINE DETECTION METHOD

To combine the advantages of the IP_CFAR and WG detectors, a proper fusion strategy is needed. Since the two energy

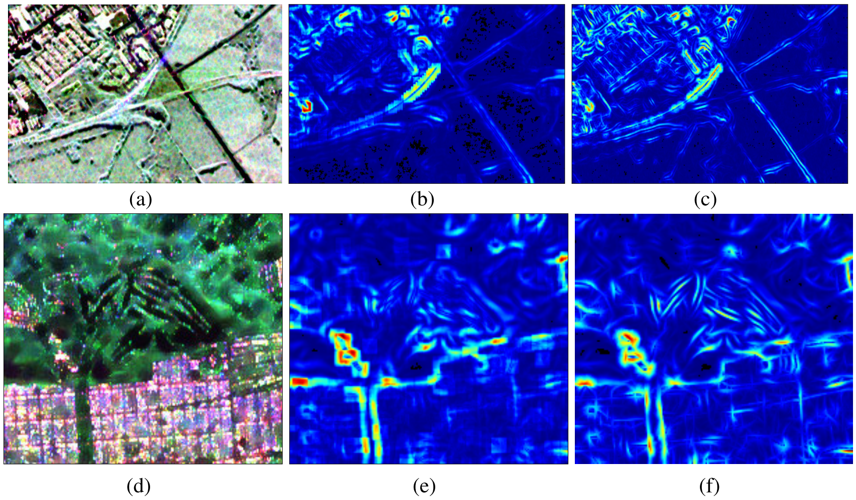

FIGURE 7. Experimental comparison of the polarimetric CFAR [16] and the proposed IP_CFAR methods. (a) PolSAR image of Ottawa; (b) edge energy map by traditional polarimetric CFAR method [16]; (c) edge energy map by proposed IP_CFAR method; (d) PolSAR subimage of San Francisco; (e) edge energy map by traditional polarimetric CFAR method [16]; (f) edge energy map by proposed IP_CFAR method.

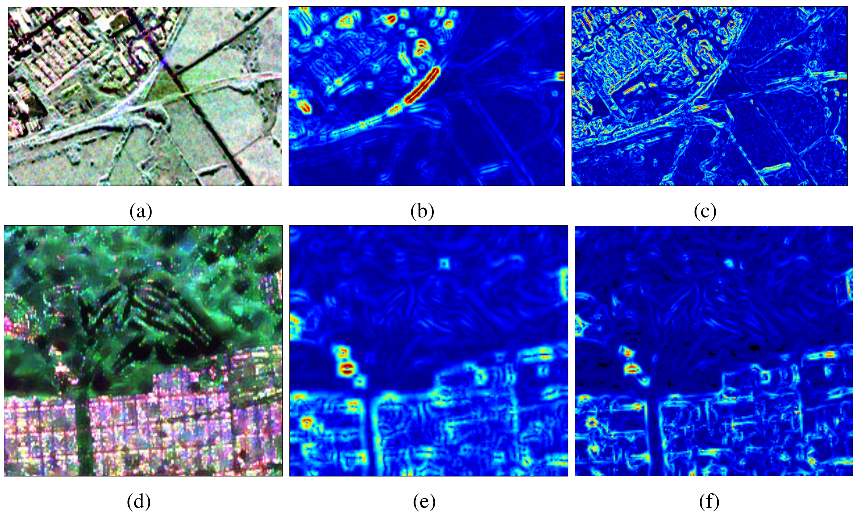

FIGURE 8. Experimental comparison of the gradient-based [16] and the proposed weighted gradient-based methods. (a) PolSAR image of Ottawa; (b) edge energy map by traditional gradient-based method [16]; (c) edge energy map by proposed WG method; (d) PolSAR subimage of San Francisco; (e) edge energy map by traditional gradient-based method [16]; (f) edge energy map by proposed WG method.

maps are obtained by different methods, it can be considered as a problem about image fusion. Image fusion aims to obtain a better image with high quality by combining complementary information from several source images so that the fused image contains more effective information and removes noises. Both the energy maps by the IP_CFAR and WG detectors are source images which should be normalized to [0, 255] in advance. The fusion objective is to produce a better energy map which can obtain large values in the edge locations of both the two energy maps and suppress other non-edge and false edge regions.

Many pixel-level image fusion methods [30], [32], [35] have been proposed in the past decades. Wavelet transform as a multi-resolution analysis approach has been widely used for image fusion [43], [44] since the image details will be separated into multiple scales and the fast algorithm is available. Since the distributions of the two energy maps are different, it is improper to fuse them directly. However, in wavelet domain, coefficients in different bands have similar distributions and can be combined directly. Therefore, a discrete stationary wavelet transform (SWT) [45] is applied to fuse the two energy maps since it is a simple and effective

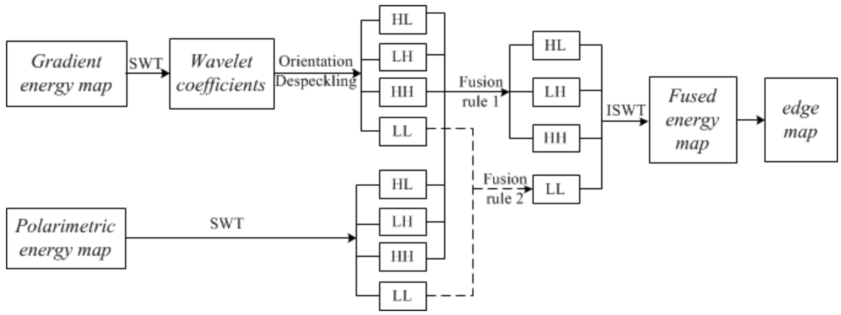

FIGURE 9. Procedure of wavelet fusion with semantic rules.

method without information loss. In addition, the gradient-based energy map has many false edges due to the speckle noises. A despeckling operation should be designed to reduce the noises. The wavelet fusion procedure is shown in Fig.9, and the main procedure of the proposed methods are given in Algorithm 1.

Algorithm 1 Hybrid Edge-Line Detection Method

1: Improved polarimetirc CFAR edge-line detection is proposed to obtain the polarimetric energy map.
2: Weighted Gradient-based edge-line detection method is designed to obtain the gradient energy map.
3: SWT is applied to the two energy maps and 3-level wavelet coefficients are obtained.
4: An orientation-based despeckling scheme is designed for the wavelet coefficients of the gradient energy map.
5: Fuse the corresponding wavelet coefficients of the two energy maps with proposed fusion rules, and inverse transform is applied to derive a fused energy map.
6: Non-maximum suppression is done and the final edge map is obtained by double thresholds.

At first, a despeckling operation is designed in wavelet domain to reduce the noises of the gradient energy map. The reason why the gradient energy map exists speckle noises are given as follows. Firstly, there are still some speckle in the PolSAR image after the refined Lee filter. In addition, due to the imaging characteristics, the scattering waves are not totally homogenous and some small variations always occur in the homogenous region. This will lead to some false edge energies in homogenous regions after the WG detector. Moreover, the WG detector cannot suppress speckle noises since the speckle in the PolSAR data is not additional. Therefore, the despeckling operation is necessary for the gradient energy map.

To suppress the noises and false edges in the gradient map, an adaptive despeckling scheme is designed by calculating the local energy [46] for wavelet coefficients. The local energy of each pixel is calculated by a set of neighborhood windows as shown in Fig. 10.The neighborhood windows consider the four directions of the high-frequency bands. Blue pixels are neighbors, while white pixels are ignored.

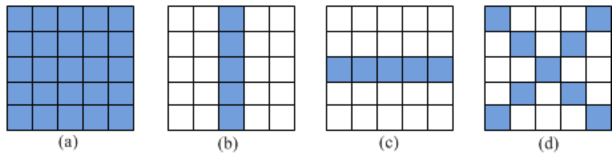

FIGURE 10. A set of neighborhood windows. (a) neighbors for LL band. (b) neighbors for HL band. (c) neighbors for LH band. (d) neighbors for HH band.

According to the orientation of each high-frequency band, different neighborhood window [47] is selected. The local energy of the low-frequency band is calculated by a 5×5 window since there is no orientation in this band. Therefore, the local energy of pixel (i, j) is defined as:

$$E(i,j) = \frac{1}{N} \sum_{(m,n)\in\eta} |F(m,n)| \tag{11}$$

where $E(i, j)$ is the local energy of the wavelet coefficient in pixel (i, j), and N is the total number of neighborhood pixels. $F(m, n)$ is the wavelet coefficient value in pixel (m, n). η is the neighborhood set obtained by the neighborhood windows in Fig.8. Fig. 8(a) is selected as the neighborhood window for the LL band. Fig. 8(b),(c) and (d) are neighborhood windows for HL, LH and HH bands respectively.

After calculating the local energies for wavelet coefficients, a despeckling scheme is used by setting a threshold of the local energies in high-frequency bands. The threshold is selected adaptively by the unsupervised method in [48]. The wavelet coefficients less than the threshold are set to zero.

The core of the image fusion is the fusion rules. Our objective is to enhance the edge information and suppress the non-edge information. Many fusion rules [49], [50] in wavelet domain have been proposed such as maximum coefficient is selected for the fused image or variances of wavelet coefficients are computed as the fused coefficients. However, an unified rule can hardly optimize contradictory objectives well since it is expected the edge information is enhanced and the background is suppressed. A simple scheme of selecting maximum values in low frequency will cause a rough background and produce false edges. Therefore, different fusion schemes should be exploited for the edge and non-edge regions.

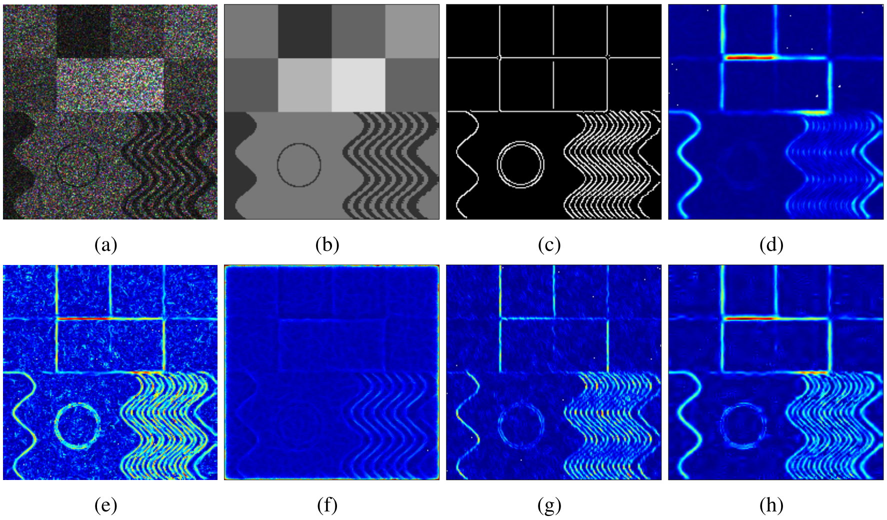

FIGURE 11. Edge detection results of the simulated PolSAR image. (a) PauliRGB image of the simulated PolSAR image; (b) the cartoon image. (c) Real edge map of the simulated PolSAR image. (d) edge map by IP_CFAR detector; (e) edge map by weighted gradient-based detector; (f) edge map by IM-NSCT method; (g) edge map by PWF-based method; (h) edge map by the proposed method.

In this paper, two different semantic rules are defined to fuse coefficients in high- and low- frequency bands. To suppress the noises, we fuse the two images by comparing their corresponding local energy values instead of the single pixel values. For coefficients in high frequency bands, the local energy maximum is selected for the fused image to enhance the edge information. For coefficients in the low frequency band, a weighted mean is used to obtain the main energy. The fusion rules can be described as follows:

$$F_{high}(i,j) = \begin{cases} F^1_{high}(i,j) & if\ E^1_{high}(i,j) \geq E^2_{high}(i,j) \\ F^2_{high}(i,j) & if\ E^1_{high}(i,j) < E^2_{high}(i,j) \end{cases} \tag{12}$$

$$F_{LL}(i,j) = \frac{E^1_{LL}(i,j)}{(E^1_{LL}(i,j)+E^2_{LL}(i,j))}F^1_{LL}(i,j) + \frac{E^2_{LL}(i,j)}{(E^1_{LL}(i,j)+E^2_{LL}(i,j))}F^2_{LL}(i,j) \tag{13}$$

where *high* includes three high frequency bands (HH,HL and LH). F_{high} and F_{LL} are the fused energy values in high and low frequency bands respectively. F^1 and F^2 represent the corresponding wavelet coefficients of the CFAR and gradient energy maps respectively. E_{LL} and E_{high} are the local energies for low- and high- frequency bands respectively.

Equation 12 is used to combine the larger energy values of high frequency bands in both CFAR and gradient images since the high frequency stands for the edge or line information. Edge energies in two images are different and complementary while both of them are in high frequency bands. Hence, the fusion scheme of selecting maximum local energy value is superior for high frequency bands. For low frequency bands, a fusion rule is proposed to obtain main information and suppress noises in Eq.(13). Weighted mean values are selected to fuse the low frequency bands since the different weights should be given for two energy maps. The weights are calculated by the ratio of their local energies, which can show their importance. After fusing Fig.2 (d) and (e), a fused energy and edge maps are shown in Figs. 2(f) and (i) respectively. It can be shown that both weak edges and structures of the urban area are enhanced simultaneously.

IV. EXPERIMENTAL STUDY

A. EXPERIMENTAL SETTINGS

In this section, four sets of simulated and real PolSAR data in different bands and sensors are used to test the effectiveness of the proposed method. The first one is the simulated PolSAR data, as shown in Fig.11(a), and its cartoon map is shown in Fig.11(b). The PolSAR data is designed as the G0 distribution in the simulated image. It is used to test the effectiveness of the proposed method in the heterogenous areas. The second one is a snythetic PolSAR image, as shown in Fig. 14(a), which is obtained from the Xi'an Area, and the corresponding edge map is shown in Fig.14(b). This synthetic PolSAR image is composed of the urban area with sharp bright-dark variations and a river with weak edges. It is used to evaluate the effectiveness of the proposed method in both the heterogenous area and the weak edge. The third one is the PolSAR image in Xi'an Area, as shown in Fig.16(a), which is RadarSAT-2 C-band fully polarimetric SAR data with the resolution of 8m. The last one is a subimage of the AIRSAR L band data in San Francisco which is 4-look fully polarimetric data. Their common characteristics are multiple of heterogeneous terrain types appearing in the PolSAR images such as buildings and forests. Moreover, the PolSAR subimage of San Francisco in Fig. 2 (a) is used to test the effectiveness of the orientation despeckling scheme in the proposed method by computing the residual SPAN image.

The parameter settings are given as follows. The filters with three scales and 18 orientations are selected for all the

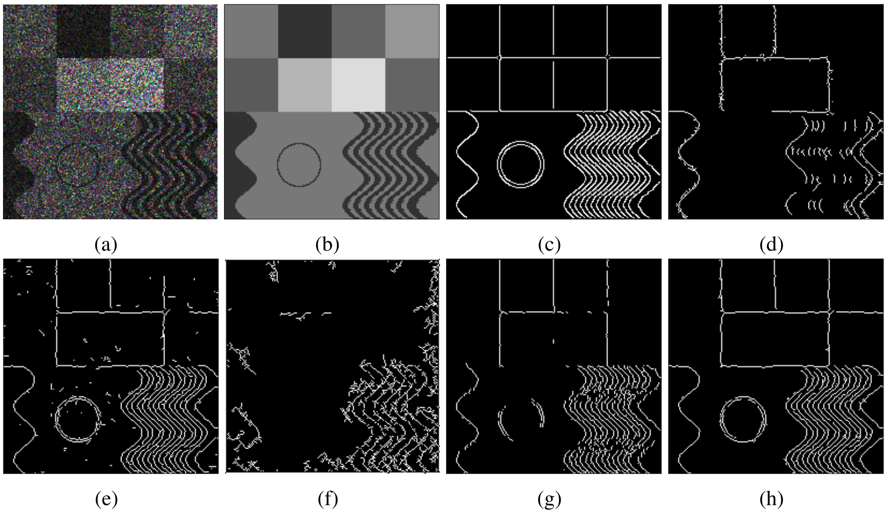

FIGURE 12. Edge detection results of the simulated PolSAR image. (a) PauliRGB image of the simulated PolSAR image; (b) the cartoon image. (c) Real edge map of the simulated PolSAR image. (d) edge map by IP_CFAR detector; (e) edge map by weighted gradient-based detector; (f) edge map by IM-NSCT method; (g) edge map by PWF-based method; (h) edge map by the proposed method.

TABLE 1. Edge accuracies of the proposed method and compared methods(%) on the simulated PolSAR image.

	IP_CFAR	Gradient	IM-NSCT	PWF	Proposed
accuracy rate	40.72	93.36	55.27	83.45	**94.46**
false alarm rate	0.77	1.03	6.08	**0.31**	0.69

experiments to better describe the edge information of various ground objects. In addition, three level wavelet transform is used to obtain multi-scale information during the wavelet fusion. The window size of the orientation despeckling operation in wavelet domain is selected as 5×5 for all the experiments. A computer with Intel Core i7 CPU and 16G RAM is used, and all the experiments are conducted on Windows system with Matlab.

Moreover, we compare the proposed method with four related edge detection methods to verify the detection performance: 1) the improved polarimetric CFAR edge detection method(IP_CFAR); 2) weighted gradient-based edge detection on SPAN images; 3) the improved multiscale edge detection method based on nonsubsampled contourlet transformation (IM-NSCT) [20] and 4) the polarimetric whitening filter (PWF)-based method [13]. Furthermore, some evaluation indexes, such as classification accuracy, confusion matrix and the ROC curve, are used to quantitatively value the proposed method and other compared methods. However, only the visual detection results are shown for the last two PolSAR images,since it is difficult to obtain the real edge maps.

B. EXPERIMENTAL RESULTS OF THE SIMULATED PolSAR IMAGE

A simulated PolSAR image with the size of 200×200 is shown in Fig. 11(a), and the corresponding cartoon image is shown in Fig. 11(b). It is composed of squares, circle and some dense curves. The real edge map, illustrated in Fig. (c), can be obtained from the cartoon image.

TABLE 2. The confusion matrix of the proposed method on the simulated PolSAR image.

	edge	non-edge
edge	3208	188
non-edge	207	36397

The edge energy maps by the four compared methods and the proposed method are shown in Fig. 11(d)-(h) respectively, and the corresponding edge maps are illustrated in Fig.12(d)-(h). We can see that the IP_CFAR detector can detect the single curve and the strong edges. It failed to detect the circle edge and the dense curves accurately since the PolSAR data donnot obey Wishart distribution. From Fig12(e), we can seen that the gradient-based detector can detect most of the intensity variation areas, but produce some speckle noises. By fusing them, the edge map by the proposed method, as shown in Fig. 12(h), can extract both the weak circle and the dense curves. The IM-NSCT method in Fig. 12(f) is difficult to detect the extreme weak edges and produce some false edges. In addition, The PWF-based method in Fig. 12 (g) also lost some square edges and the dense curves.

To evaluate quantitatively of the extracted edges, edge accuracies of the proposed and compared methods are given in Table 1. The threshold is selected adaptively by the OTSU

TABLE 3. Running time of the proposed method and compared methods(s) on the simulated PolSAR image.

	IP_CFAR	Gradient	IM-NSCT	PWF	Proposed
executed time	385.69	66.43	**15.98**	18.95	516.82

TABLE 4. Edge accuracies of the proposed method and compared methods(%) on the synthetic PolSAR image.

	IP_CFAR	Gradient	IM-NSCT	PWF	Proposed
accuracy rate	35.63	60.73	68.63	71.66	**89.68**
false alarm rate	2.57	2.73	3.43	**2.17**	2.75

method [48]. It is considered that a superior edge detection method should have higher accuracy rate and lower false alarm rate. It can been seen that the proposed method have 53.74%,1.1%,39.19%,11.01% higher edge accuracy rate than four compared methods. In addition, the false alarm rate of the proposed method is lower than most of compared methods.

In addition, the confusion matrix of the proposed method is calculated in Table 2. There are totally 40000 pixels in Fig. 11 (a), in which the numbers of the edge and non-edge pixels are 3396 and 36604 respectively. It can be seen that most of the edge pixels can be detected correctly, and the main error is that some edge pixels are detected as non-edges. It is because the extremely weak edges are difficult to be extracted.

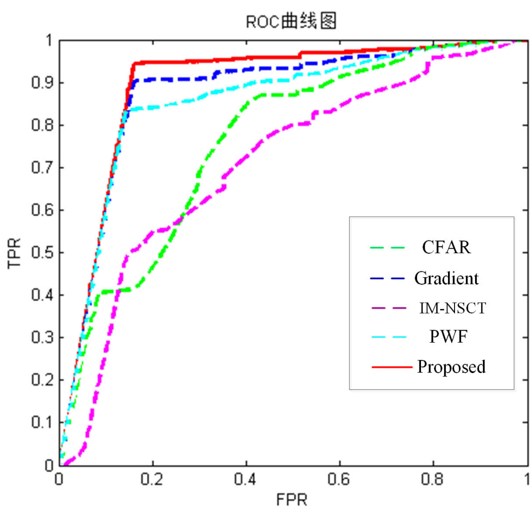

FIGURE 13. ROC curves on the simulated image.

Moreover, receiver operating characteristic (ROC) curve, illustrated in Fig. 13, is used to evaluate quantitatively the performance of the proposed method and other compared methods. The x-axis represents the false positive rate (FPR), and the y-axis is the true positive rate (TPR). The true-positive rate is also known as sensitivity, recall or probability of detection [51] in machine learning. The false-positive rate is also known as the fall-out or probability of false alarm [51]. Better performance is obtained if the ROC curve is closer the top left corner. The proposed method is the red curve and the four compared methods are represented by other color curves. It can be seen that the proposed method can obtain better performance than other methods.

What is more, the running time is computed for the proposed and other compared methods shown in Table 3. It can be seen the IP_CFAR and the proposed methods cost more time than other methods. There are mainly two reasons. One is that edge and line filters with 3 scales and 18 directions are calculated for each pixel. In other words, during edge-line detection, 108 filters will be applied to each pixel. Another reason is that the Wishart distance, which includes the matrix inverse and trace operations, will be calculated during each edge-line filtering. And matrix inverse and trace operations are time costing. Moreover, the proposed method spends most time, since it needs to fuse the IP_CFAR and WG methods. The most time is spent on the IP_CFAR detector due to the matrix operation. However, the proposed method can obtain superior performance.

C. EXPERIMENTAL RESULTS OF THE SYNTHETIC PolSAR IMAGE

A synthetic Pauli RGB image is shown in Fig. 14(a). It is obtained by selecting two blocks of Xi'an area. One is the urban area and another is the river in the rectangles in Fig. 16(a). It is designed to test whether the proposed method can detect both sharp variations in the urban area and weak edges along the river or not. Fig. 14(b) is the true edge map. Fig. 14(c) is obtained by mapping the true edge map to SPAN image of Fig. 14(a).

The edge maps by the four compared methods and the proposed method are shown in Fig. 14(d)-(h) respectively. We can see that the IP_CFAR detector can detect the edges between two different terrain types well especially the weak edges along the river. Moreover, the gradient-based detector can obtain more detailed edges in the urban area. By fusing them, the edge map by the proposed method is shown Fig. 14(h). It can be seen that the fused edge map can extract both the details in the urban area and the weak edges. The compared IM-NSCT method in Fig. 14(f) cannot suppress the speckle noises and produces some false edges. The PWF-based method in Fig. 14(g) loses some details in the urban area.

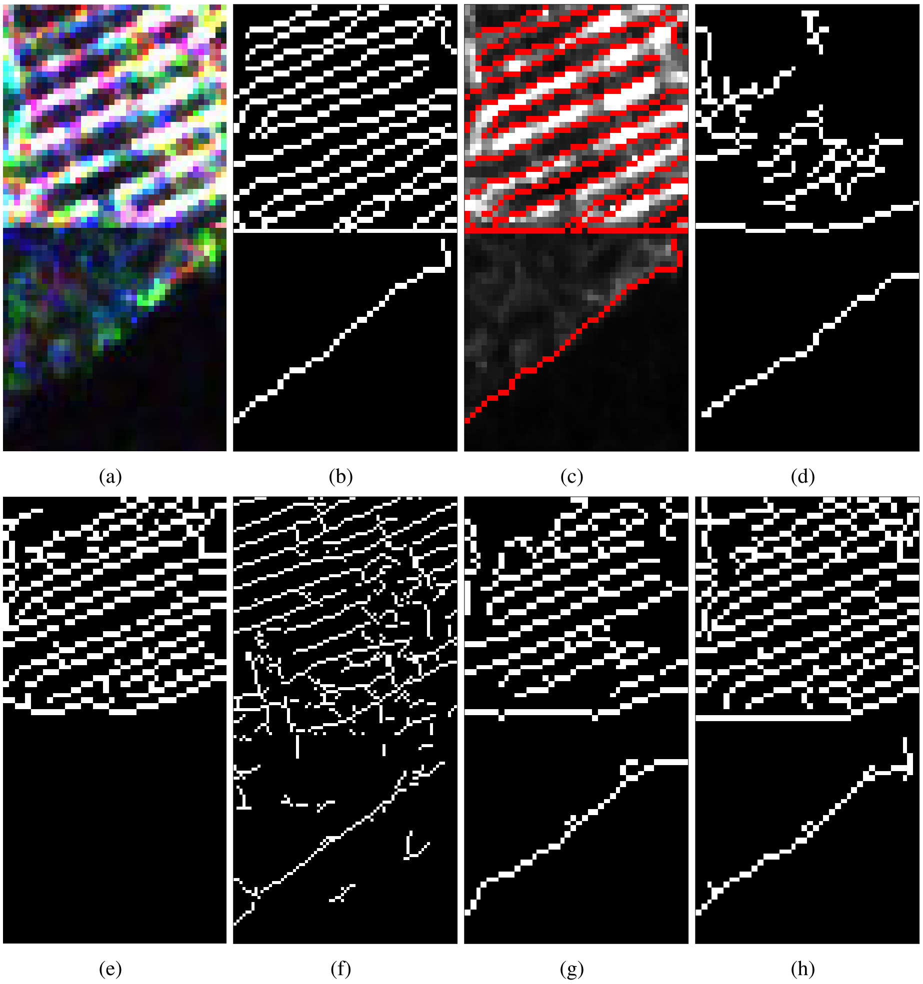

FIGURE 14. Edge detection results of the synthetic PolSAR image. (a) pseudo color image of the synthetic PolSAR image; (b) true edge map. (c) mapping edges to SPAN image. (d) edge map by IP_CFAR detector; (e) edge map by weighted gradient-based detector; (f) edge map by IM-NSCT method; (g) edge map by PWF-based method; (h) edge map by the proposed method.

TABLE 5. The confusion matrix of the proposed method on the synthetic PolSAR image.

	edge	non-edge
edge	443	50
non-edge	91	2666

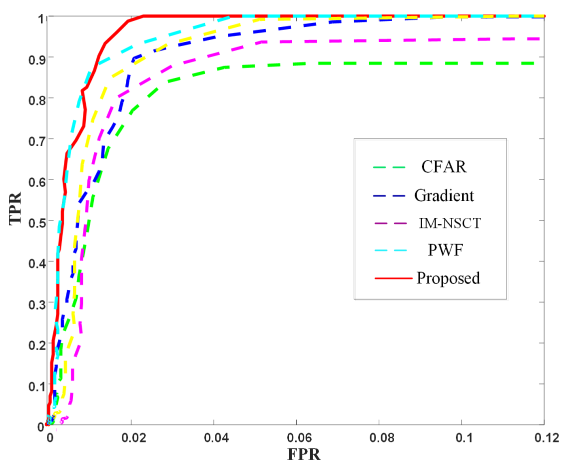

FIGURE 15. ROC curves on the synthetic image.

To evaluate quantitatively of the extracted edges, edge accuracies of the proposed and compared methods in Fig. 14 are given in Table 4. It can been seen that the proposed method have 54.05%,28.95%,21.05%,18.02% higher edge accuracy rate than four compared methods. In addition, the false alarm rates of these methods are similar and not too high. The false edges by the proposed method is produced since the left and right sides of the urban area are confused by speckle noises, and the edges are hardly to be distinguished. It is considered that more excellent despecking method needs to be designed for PolSAR image in the further work, such as shearlet-based despeckling for SAR images [52].

In addition, the confusion matrix of the proposed method is calculated in Table 5. There are totally 3200 pixels in Fig. 14 (a), in which the numbers of the edge and non-edge pixels are 493 and 2707 respectively. It can be seen that most of the edge pixels can be detected correctly, and the main

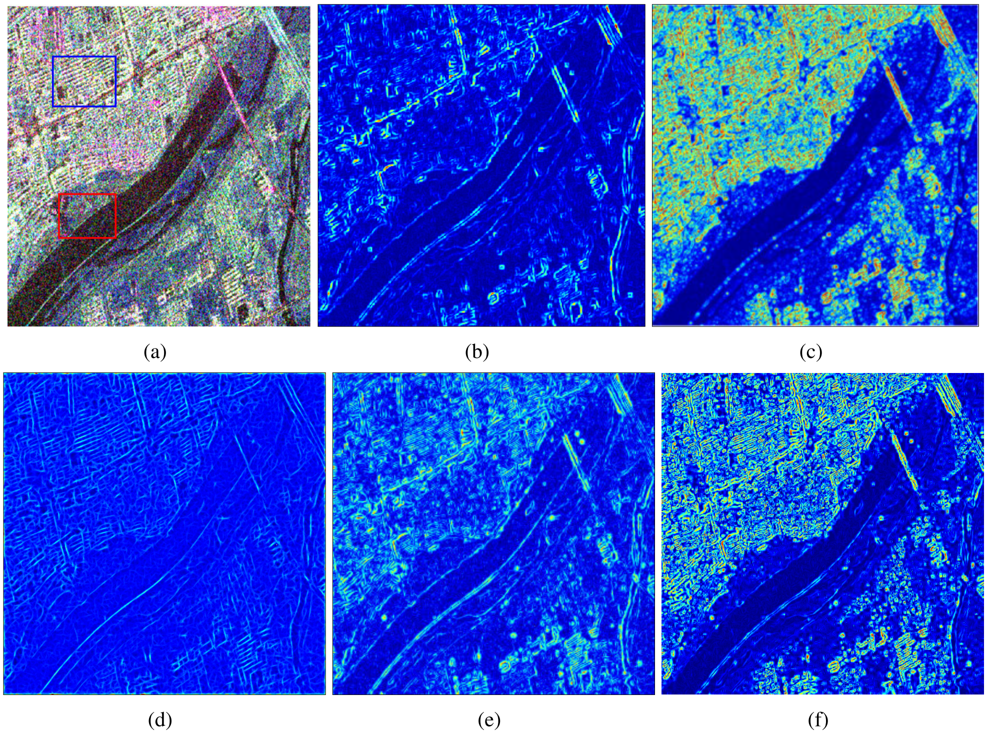

FIGURE 16. Edge energy maps of the Xi'an area. (a) pseudo color image of Xi'an area; (b) energy map by IP_CFAR detector; (c) energy map by weighted gradient-based detector; (d) energy map by IM-NSCT method; (e) energy map by PWF-based method; (f) energy map by the proposed method.

error is that more pixels are detected as edges. Changing threshold may produce a better result. A better threshold selection method can be studied in the further work.

Moreover, receiver operating characteristic (ROC) curve, illustrated in Fig. 15, is used to evaluate quantitatively the performance of the proposed method and other compared methods. The x-axis represents the false positive rate (FPR), and the y-axis is the true positive rate (TPR). Better performance is obtained if the ROC curve is closer the top left corner. The proposed method is the red curve and the four compared methods are represented by other color curves. It can be seen that the proposed method can obtain better performance than other methods.

D. EXPERIMENTAL RESULTS OF XI'AN AREA DATA SET

The pseudo color image of Xi'an area is shown in Fig. 16(a) with the size of 512×512. There are the buildings on the left-up corner, and a river along the urban area. Cross the river, there are three bridges on the right-up corner and a railway parallel to the bridge. In addition, there are some villages and the bare soil on the right-down corner. Another small river is laid on the right of the image. There are lots of details and edges in this image. This is a complex scene of the PolSAR image with various ground objects, and it is a difficult task to detect all the edges.

The edge energy maps by the four compared methods and the proposed method are illustrated in Fig.16(b)-(f) respectively. The polarimetric and gradient-based energy maps are shown in Fig. 16(b) and (c) respectively. We can see that the IP_CFAR detector can obtain many edges between two different terrain types especially the weak edges along the river. However, it is not sensitive to the edges in the heterogenous urban area. Moreover, the gradient-based detector can obtain many details especially the edges in the urban area while it is difficult to detect the weak edges. By fusing them, the edge energy by the proposed method is shown Fig. 16(f). It can be seen that the fused energy map have both the details and the weak edges. Moreover, the noises in the gradient energy map are suppressed in Fig. 16(f). Two other compared methods are shown in Fig. 16(d) and (e). It can be seen the compared methods still produce speckle noises especially in the river area.

According to the energy maps, a non-maximum suppression method is applied to obtain the edge maps. The edge maps of the compared and proposed methods are given in Fig. 17(b)-(f) respectively. It can be seen that the edge maps obtain similar results as the energy maps. The IP_CFAR detector in (b) can detect weak edges along the river well, while it cannot detect the edges in the urban area. The gradient-based detector can detect the edges in the urban area while it loses the edges along the river. The IM-NSCT and PWF-based methods can detect the heterogenous area and the weak edges well. However, they are sensitive to the noises and produce some false edges. The proposed method can not

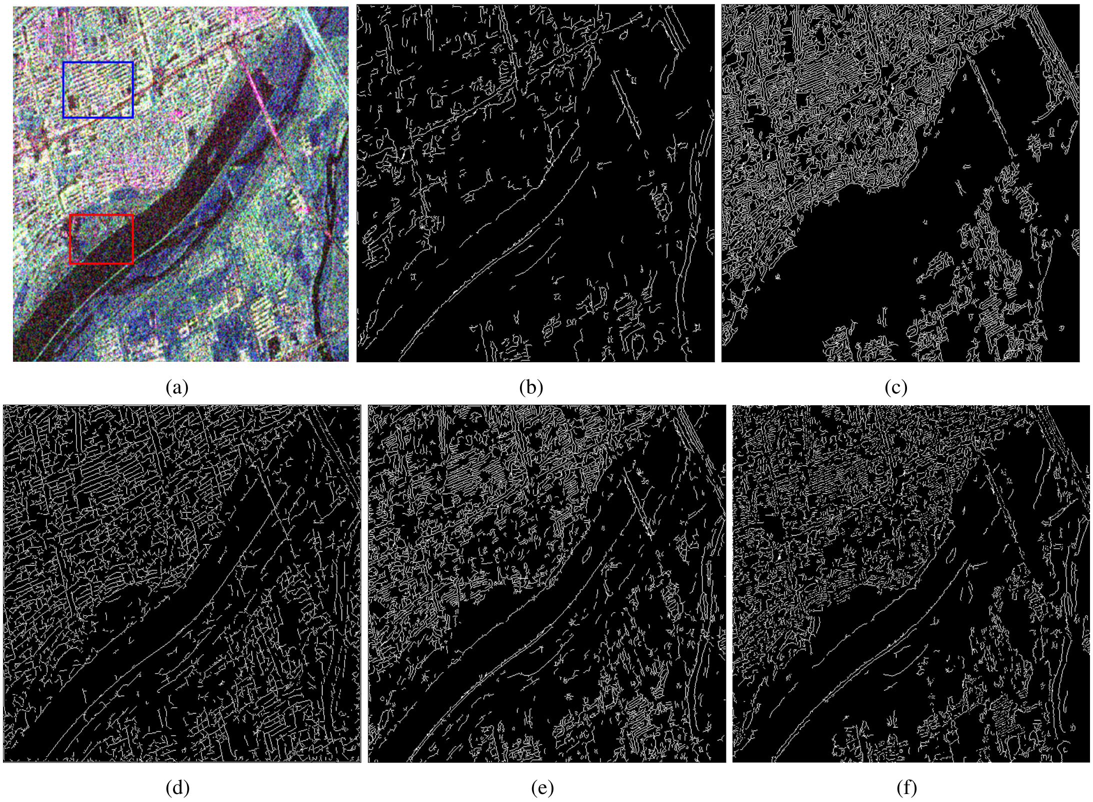

FIGURE 17. Edge detection results of the Xi'an area. (a) pseudo color image of Xi'an area; (b) edge map by IP_CFAR detector; (c) edge map by weighted gradient-based detector; (d) edge map by IM-NSCT method; (e) edge map by PWF-based method; (f) edge map by the proposed method.

only detect heterogenous areas and weak edges well, but also suppress the speckle noises.

E. EXPERIMENTAL RESULTS OF SAN FRANCISCO DATA SET 1

A subimage of San Francisco data is used with the size of 180×200. Its pseudo color image is shown in Fig. 18(a) with Pauli base as the RGB channels. This image mainly includes the urban area and the forest, and a golf filed was built in the forest.

The edge energy maps by the four compared and proposed methods are illustrated in Fig. 18(b)-(f) respectively. It can be seen that the IP_CFAR detector in Fig.18(b) can detect weak edges well especially for the edges of the golf filed, but it is not sensitive to the edges in the heterogenous urban area. On the contrary, the gradient-based detector in Fig.18(c) can obtain large edge energies especially in the urban area while it losed the edges in the golf filed. Two other compared methods are shown in Fig. 18(d) and (e) after the logarithmic transformation. It can be seen the other two methods still produce speckle noises especially in the forest. In Fig. 18(f), the edge energy by proposed method shows obvious improvement by combining the advantages of the IP_CFAR and gradient-based detectors. Our method can detect both the details in the urban area and the weak edges in the golf filed well, and the noises are suppressed in Fig. 18(f) either.

In addition, the final edge maps by the four compared methods and the proposed method are shown in Fig. 19(b)–(f) respectively. It can be seen that the IP_CFAR detector can detect the weak edge well such as the golf field in the forest. However, it cannot detect the sharp bright-dark variation caused by the building and the thin road in the urban area. Contrary to the IP_CFAR detector, the WG detector can detect the urban area well but fail to detect the weak edges. Two other compared methods are shown in Figs. 19(d) and (e). It can be seen that they can detect the weak edges and the urban areas but are sensitive to the speckle noises, and obtain some false edges in the urban area and the forest. By contrast, the proposed method in Fig. 19(f) not only keeps the weak edges from the IP_CFAR detector but also obtains the edge in the urban area. In addition, the noises are suppressed in the fused edge map.

F. EXPERIMENTAL RESULTS OF SAN FRANCISCO DATA SET 2

In this paper, an adaptive despeckling operation is designed in wavelet domain to reduce the noises of the gradient energy map. To test the effectiveness of the proposed despeckling method, the San Francisco subimage is used as shown in Fig. 2(a). Its corresponding SPAN image is shown in Fig. 20(a) after the refined Lee filter. Fig.20 (b) is the

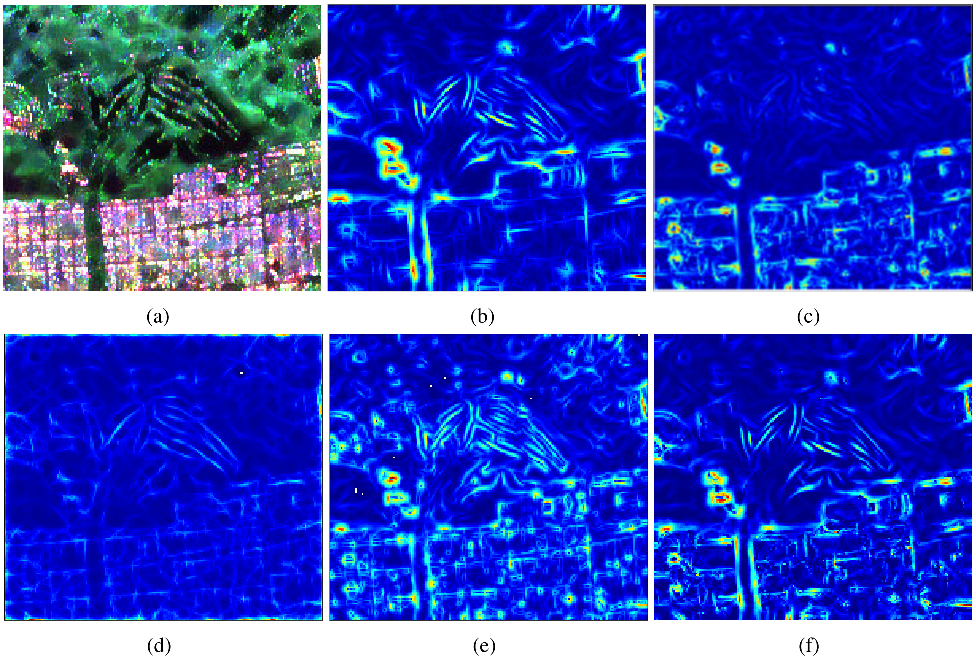

FIGURE 18. Edge detection results of the San Francisco area. (a) pseudo color image of San Francisco area; (b) energy map by IP_CFAR detector; (c) energy map by weighted gradient-based detector; (d) energy map by IM-NSCT method; (e) energy map by PWF-based method; (f) energy map by the proposed method.

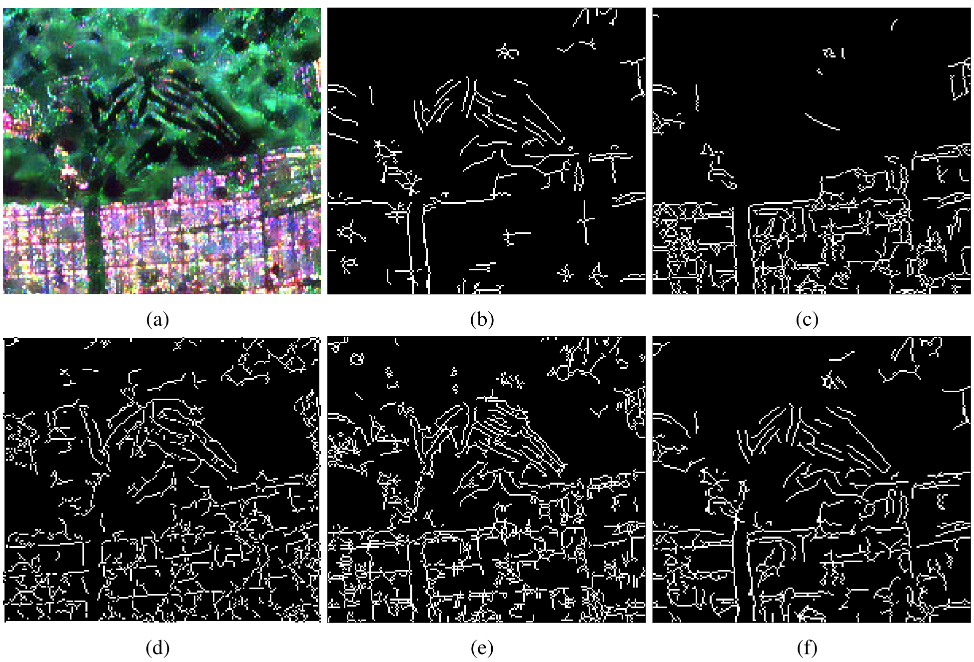

FIGURE 19. Edge detection results of the San Francisco area. (a) pseudo color image of San Francisco area; (b) edge map by IP_CFAR detector; (c) edge map by weighted gradient-based detector; (d) edge map by IM-NSCT method; (e) edge map by PWF-based method; (f) edge map by the proposed method.

gradient energy map. It can be seen that some noises appear in the forest. After the despeckling operation in wavelet domain, the obtained gradient energy maps by using different filtering windows with $3 \times 3 \sim 9 \times 9$ are shown in Figs. 20(c)-(f) respectively. Since the despeckling operation is conducted along the direction in high-frequency bands, filtering windows with different size can obtain similar results. All of them can suppress the noises and keep original signal well. The residuals are shown in Fig.21 with different window size. It illustrates that the residuals are similar and no edge

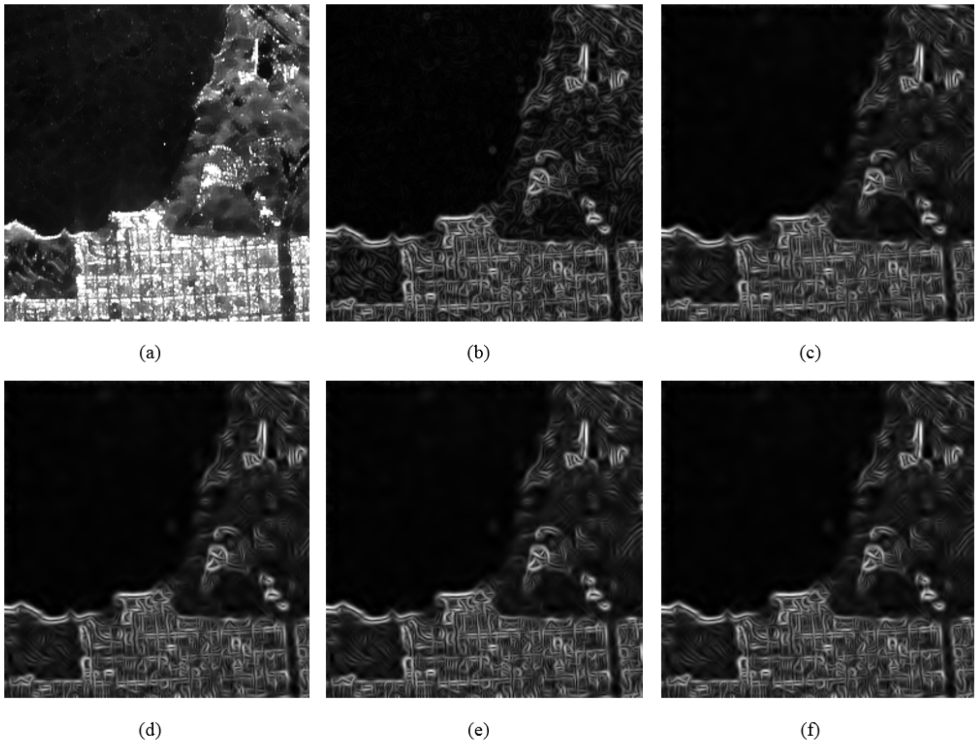

FIGURE 20. Experimental results by the despeckling operation with different windows. (a) SPAN image of San Francisco. (b)Gradient energy map; (c) 3 × 3; (d) 5 × 5; (e) 7 × 7;(f) 9 × 9.

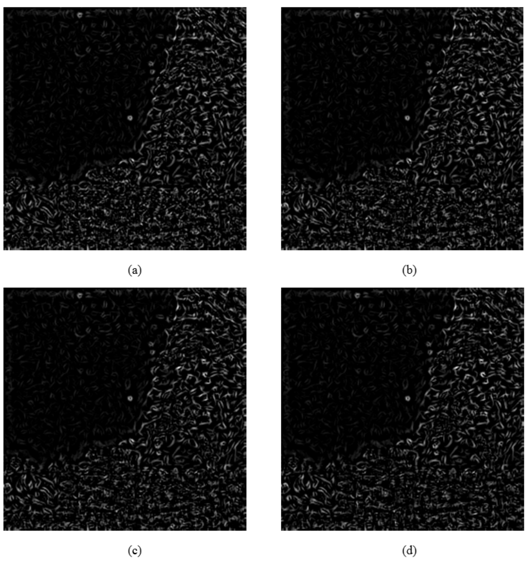

FIGURE 21. Residual SPAN images with different filtering windows. (a) 3 × 3; (b) 5 × 5; (c) 7 × 7;(d) 9 × 9.

information are suppressed. It verifies that the despeckling operation is robust to window size and can control signal loss well. In general, we choose 5 as the window size.

V. CONCLUSION

In this paper, a hybrid edge detection method is presented to fuse the advantages of two detectors, which are the proposed IP_CFAR and WG detectors. For the first detector, according to the the limitation of Wishart measurement and traditional filter configuration in the CFAR detector, an IP_CFAR detector is designed to detect weak edges well. For the second one, the WG detector is designed to detect the strong intensity changes in the heterogenous areas. Then, a hybrid edge detection method is proposed by combining the merits of the two detectors above. Wavelet fusion is designed and different semantic rules are defined to fuse high-frequency and low-frequency wavelet sub-bands respectively. Moreover, a despeckling method is proposed to suppress the noises in the gradient energy map. Several experiments are conducted on simulated and real PolSAR data, and they show the effectiveness of the proposed method.

In addition, the proposed method gives a novel framework for PolSAR edge detection. Traditional edge detection method is trying to design a better detector. However, no one method can detect all the edges well for various terrain types. In this paper, we proposed a novel hybrid framework by fusing two detectors with wavelet transform. By this, the proposed method is superior to both methods. It validates the statement that one plus one is greater than two.

Furthermore, the proposed method is not limited to the two detectors, and it can fuse any two methods as long as they can provide complementary information. Therefore, this paper gives a novel framework to improve the edge detection result. This framework can also extend to image classification, object recognition and so forth. In the further work, we will try to improve its commonality by fusing more detectors. Moreover, more effective despeckling method should be proposed to improve the fusion result.

REFERENCES

[1] H. Bi, J. Sun, and Z. Xu, "A graph–based semisupervised deep learning model for PolSAR image classification," *IEEE Trans. Geosci. Remote Sens.*, vol. 57, no. 4, pp. 2116–2132, Apr. 2019.

[2] F. Liu, L. Jiao, and X. Tang, "Task–oriented GAN for PolSAR image classification and clustering," *IEEE Trans. Neural Netw. Learn. Syst.*, vol. 30, no. 9, pp. 2707–2719, Sep. 2019.

[3] D. Yang, L. Du, H. Liu, Y. Wang, and M. Gu, "Extended geometrical perturbation based detectors for PolSAR image target detection in heterogeneously patched regions," *IEEE J. Sel. Topics Appl. Earth Observ. Remote Sens.*, vol. 12, no. 1, pp. 285–301, Jan. 2019.

[4] W. Liu, J. Yang, J. Zhao, H. Shi, and L. Yang, "An unsupervised change detection method using time–series of PolSAR images from Radarsat–2 and GaoFen–3," *Sensors*, vol. 18, no. 2, p. 559, Feb. 2018.

[5] L. Wang, X. Xu, H. Dong, R. Gui, and F. Pu, "Multi–pixel simultaneous classification of PolSAR image using convolutional neural networks," *Sensors*, vol. 18, no. 3, p. 769, Mar. 2018.

[6] J.-F. Shi, F. Liu, Y.-H. Lin, and L. Liu, "Polarimetric SAR image classification based on deep learning and hierarchical semantic model," *Acta Automatica Sinica*, vol. 43, no. 2, pp. 215–226, 2017.

[7] W. Chen, S. Gou, X. Wang, L. Jiao, C. Jiao, and A. Zare, "Complex scene classification of PoLSAR imagery based on a self–paced learning approach," *IEEE J. Sel. Topics Appl. Earth Observ. Remote Sens.*, vol. 11, no. 12, pp. 4818–4825, Dec. 2018.

[8] J. Xie, Z. Li, C. Zhou, Y. Fang, and Q. Zhang, "Speckle filtering of GF–3 polarimetric SAR data with joint restriction principle," *Sensors*, vol. 18, no. 5, p. 1533, May 2018.

[9] G. Zhou, Y. Cui, Y. Chen, and J. Yang, "A new edge detection method of polarimetric SAR images using the curvelet transform and the Duda operator," in *Proc. IET Conf. Publications*, 2009, pp. 1–9.

[10] G. Zhou, Y. Cui, Y. Chen, J. Yang, H. Rashvand, and Y. Yamaguchi, "Linear feature detection in polarimetric SAR images," *IEEE Trans. Geosci. Remote Sens.*, vol. 49, no. 4, pp. 1453–1463, Apr. 2011.

[11] X. You, Q. Li, D. Tao, W. Ou, and M. Gong, "Local metric learning for exemplar–based object detection," *IEEE Trans. Circuits Syst. Video Technol.*, vol. 24, no. 8, pp. 1265–1276, Aug. 2014.

[12] S. Deng, J. Zhang, P. Li, and J. Yang, "Edge detection for polarimetric SAR images combining adaptive optimal polarimetric contrast enhancement and ROA operator," in *Proc. IET Int. Radar Conf.*, 2013, pp. 1–6.

[13] S. Deng, J. Zhang, P. Li, and G. Huang, "Edge detection from polarimetric SAR images using polarimetric whitening filter," in *Proc. IEEE Int. Geosci. Remote Sens. Symp.*, Jul. 2011, pp. 448–451.

[14] S. Deng, J. Zhang, and P. Li, "Improved polarimetric whitening filter for edge detection," *J. Image Graph.*, vol. 17, no. 5, pp. 665–670, 2012.

[15] R. G. Caves and S. Quegan, "Multichannel SAR segmentation: Algorithms and applications," in *Proc. Synth. Aperture Radar Passive Microw. Sens.*, Nov. 1995, pp. 1–6.

[16] J. Schou, H. Skriver, A. Nielsen, and K. Conradsen, "CFAR edge detector for polarimetric SAR images," *IEEE Trans. Geosci. Remote Sens.*, vol. 41, no. 1, pp. 20–32, Jan. 2003.

[17] X. Ma, S. Liu, S. Hu, P. Geng, M. Liu, and J. Zhao, "SAR image edge detection via sparse representation," *Soft Comput.*, vol. 22, no. 8, pp. 2507–2515, Apr. 2018.

[18] S. Yi, D. Labate, G. Easley, and H. Krim, "A shearlet approach to edge analysis and detection," *IEEE Trans. Image Process.*, vol. 18, no. 5, pp. 929–941, May 2009.

[19] M. A. Duval-Poo, F. Odone, and E. De Vito, "Edges and corners with shearlets," *IEEE Trans. Image Process.*, vol. 24, no. 11, pp. 3768–3780, Nov. 2015.

[20] R. Jin, J. Yin, W. Zhou, and J. Yang, "Improved multiscale edge detection method for polarimetric SAR images," *IEEE Geosci. Remote Sens. Lett.*, vol. 13, no. 8, pp. 1104–1108, Aug. 2016.

[21] W. Xie, L. Jiao, and J. Zhao, "PolSAR image classification via D–KSVD and NSCT–domain features extraction," *IEEE Geosci. Remote Sens. Lett.*, vol. 13, no. 2, pp. 227–231, Feb. 2016.

[22] H. Yi, J. Yang, P. Li, L. Shi, and F. Lang, "A PolSAR image segmentation algorithm based on scattering characteristics and the revised wishart distance," *Sensors*, vol. 18, no. 7, p. 2262, Jul. 2018.

[23] H. Yan, Z. Shan, and F. Gao, "Edge detection algorithm for SAR image based on enhanced ROEWA," *J. Electron. Inf. Technol.*, vol. 40, no. 5, pp. 1166–1172, 2018.

[24] G. Liu, L. Jiao, F. Liu, H. Zhong, and S. Wang, "A new patch based change detector for polarimetric SAR data," *Pattern Recognit.*, vol. 48, no. 3, pp. 685–695, Mar. 2015.

[25] D. Xiang, Y. Ban, W. Wang, T. Tang, and Y. Su, "Edge detector for polarimetric SAR images using SIRV model and gauss–shaped filter," *IEEE Geosci. Remote Sens. Lett.*, vol. 13, no. 11, pp. 1661–1665, Nov. 2016.

[26] D. Xiang, Y. Ban, W. Wang, and Y. Su, "Adaptive superpixel generation for polarimetric SAR images with local iterative clustering and SIRV model," *IEEE Trans. Geosci. Remote Sens.*, vol. 55, no. 6, pp. 3115–3131, Jun. 2017.

[27] W. Wang, D. Xiang, Y. Ban, J. Zhang, and J. Wan, "Enhanced edge detection for polarimetric SAR images using a directional span-driven adaptive window," *Int. J. Remote Sens.*, vol. 39, no. 19, pp. 6340–6357, Oct. 2018.

[28] W. Wang, J. Ou, J. Zhang, and J. Wan, "Edge detection for polarimetric SAR images using span-driven adaptive filter," in *Proc. IEEE Radar Conf. (RadarConf)*, May 2017, pp. 1099–1102.

[29] B. Liu, Z. Zhang, X. Liu, and W. Yu, "Edge extraction for polarimetric SAR images using degenerate filter with weighted maximum likelihood estimation," *IEEE Geosci. Remote Sens. Lett.*, vol. 11, no. 12, pp. 2140–2144, Dec. 2014.

[30] J. Wu, F. Liu, L. Jiao, X. Zhang, H. Hao, and S. Wang, "Local maximal homogeneous region search for SAR speckle reduction with sketch–based geometrical kernel function," *IEEE Trans. Geosci. Remote Sens.*, vol. 52, no. 9, pp. 5751–5764, Sep. 2014.

[31] P. Shen, C. Wang, H. Gao, and J. Zhu, "An adaptive nonlocal mean filter for PolSAR data with shape–adaptive patches matching," *Sensors*, vol. 18, no. 7, p. 2215, Jul. 2018.

[32] F. Liu, J. Shi, L. Jiao, H. Liu, S. Yang, J. Wu, H. Hao, and J. Yuan, "Hierarchical semantic model and scattering mechanism based PolSAR image classification," *Pattern Recognit.*, vol. 59, pp. 325–342, Nov. 2016.

[33] M. Mahdianpari, B. Salehi, and F. Mohammadimanesh, "A new speckle reduction algorithm of polsar images based on a combined Gaussian random field model and wavelet edge detection approach," in *Proc. IEEE Int. Geosci. Remote Sens. Symp. (IGARSS)*, Jul. 2017, pp. 2349–2352.

[34] H. Wu and Y. Xing, "Pixel-based image fusion using wavelet transform for SPOT and ETM+ image," in *Proc. IEEE Int. Conf. Prog. Inform. Comput.*, Dec. 2010, pp. 936–940.

[35] G. Piella, "A general framework for multiresolution image fusion: From pixels to regions," *Inf. Fusion*, vol. 4, no. 4, pp. 259–280, Dec. 2003.

[36] H. Liu, Z. He, Y. Zhao, J. Teng, Y. Wang, H. Liu, Z. He, Y. Zhao, J. Teng, and Y. Wang, "Improved ROEWA edge detector for SAR images," *J. Remote Sens.*, vol. 21, no. 2, pp. 273–279, 2017.

[37] Y. Zheng, L. Jiao, H. Liu, X. Zhang, B. Hou, and S. Wang, "Unsupervised saliency-guided SAR image change detection," *Pattern Recognit.*, vol. 61, pp. 309–326, Jan. 2017.

[38] Z. Liu and H. Xu, "Image denoising with nonsubsampled wavelet–based contourlet transform," in *Proc. 5th Int. Conf. Fuzzy Syst. Knowl. Discovery*, Oct. 2008, pp. 301–305.

[39] J.-S. Lee and E. Pottier, *Polarimetric Radar Imaging: From Basics to Applications*. Boca Raton, FL, USA: CRC Press, 2009.

[40] K. Conradsen, A. Nielsen, J. Schou, and H. Skriver, "A test statistic in the complex wishart distribution and its application to change detection in polarimetric SAR data," *IEEE Trans. Geosci. Remote Sens.*, vol. 41, no. 1, pp. 4–19, Jan. 2003.

[41] J.-S. Lee, M. Grunes, and G. de Grandi, "Polarimetric SAR speckle filtering and its implication for classification," *IEEE Trans. Geosci. Remote Sens.*, vol. 37, no. 5, pp. 2363–2373, Sep. 1999.

[42] Y. Yamaguchi, Y. Yajima, and H. Yamada, "A four–component decomposition of POLSAR images based on the coherency matrix," *IEEE Geosci. Remote Sens. Lett.*, vol. 3, no. 3, pp. 292–296, Jul. 2006.

[43] M. Gong, Z. Zhou, and J. Ma, "Change detection in synthetic aperture radar images based on image fusion and fuzzy clustering," *IEEE Trans. Image Process.*, vol. 21, no. 4, pp. 2141–2151, Apr. 2012.

[44] J. Ma, M. Gong, and Z. Zhou, "Wavelet fusion on ratio images for change detection in SAR images," *IEEE Geosci. Remote Sens. Lett.*, vol. 9, no. 6, pp. 1122–1126, Nov. 2012.

[45] H. Choi and J. Jeong, "Despeckling images using a preprocessing filter and discrete wavelet transform–based noise reduction techniques," *IEEE Sensors J.*, vol. 18, no. 8, pp. 3131–3139, Apr. 2018.

[46] G. Chen and X. Liu, "Wavelet-based despeckling SAR images using neighbouring wavelet coefficients," in *Proc. IEEE Int. Geosci. Remote Sens. Symp. (IGARSS)*, Nov. 2005, pp. 1764–1766.
[47] J. Shi, L. Li, F. Liu, L. Jiao, H. Liu, S. Yang, L. Liu, and H. Hao, "Unsupervised polarimetric synthetic aperture radar image classification based on sketch map and adaptive Markov random field," *J. Appl. Remote Sens*, vol. 10, no. 2, May 2016, Art. no. 025008.
[48] N. Otsu, "A threshold selection method from gray–level histograms," *IEEE Trans. Syst., Man, Cybern., Syst.*, vol. 9, no. 1, pp. 62–66, Jan. 1979.
[49] O. Prakash, R. Srivastava, and A. Khare, "Biorthogonal wavelet transform based image fusion using absolute maximum fusion rule," in *Proc. IEEE Conf. Inf. Commun. Technol.*, Apr. 2013, pp. 577–582.
[50] S. Roy, P. Shivakumara, P. P. Roy, and C. L. Tan, "Wavelet-gradient-fusion for video text binarization," in *Proc. 21st Int. Conf. Pattern Recognit.*, Nov. 2012, pp. 3300–3303.
[51] S. Alam, O. Olabiyi, O. Odejide, and A. Annamalai, "Simplified performance analysis of energy detectors over myriad fading channels: Area under the ROC curve approach," *Int. J. Wireless Mobile Netw.*, vol. 4, no. 4, pp. 33–52, Aug. 2012.
[52] S. Liu, M. Shi, S. Hu, and Y. Xiao, "Synthetic aperture radar image denoising based on Shearlet transform using the context-based model," *Phys. Commun.*, vol. 13, pp. 221–229, Dec. 2014.

JUNFEI SHI received the B.S. degree in computer science and technology from Henan Normal University, Henan, China, in 2009, and the Ph.D. degree in computer science and technology from Xidian University, Xi'an, China, in 2016. She is currently a Faculty Member with the School of Computer Science and Engineering, Xi'an University of Technology, Xi'an. Her current research interests include polarimetric SAR image classification, semantic model, and computer vision.

HAIYAN JIN received the B.S. degree from Xi'an Shiyou University, Xi'an, China, in 1999, and the M.S. and Ph.D. degrees from Xidian University, Xi'an, in 2005 and 2007, respectively. She is currently with the Xi'an University of Technology, Xi'an. She has published more than 30 articles in journals and international conferences. Her interests include intelligent information processing, image processing, and pattern recognition.

ZHAOLIN XIAO received the Ph.D. degree from Northwestern Polytechnical University, in 2014. He is currently an Associate Professor with the Department of Computer Science and Engineering, Xi'an University of Technology. His research interests include computer vision and computational photography.

• • •